ELSEVIER

Polymer 43 (2002) 7345–7365

polymer

www.elsevier.com/locate/polymer

HDPE/LLDPE reactor blends with bimodal microstructures—part I: mechanical properties

Colin Li Pi Shan, João B. P. Soares*, Alexander Penlidis

Department of Chemical Engineering, Institute for Polymer Research, University of Waterloo, Waterloo, Ont., Canada N2L 3G1

Received 15 March 2002; received in revised form 17 September 2002; accepted 19 September 2002

Abstract

Reactor blends of polyethylene/poly(ethylene-*co*-1-octene) resins with bimodal molecular weight and bimodal short chain branching distributions were synthesized in a two-step polymerization process. The compositions of these blends range from low molecular weight (LMW) homopolymer to high molecular weight (HMW) copolymer and, vice versa, HMW homopolymer to LMW copolymer. The physical properties of the blends were found to be consistent with the nature of the individual components. For the tensile properties, the stiffness decreases with increasing the fraction of the copolymer, regardless of the molecular weight of the homopolymer fraction. For these blends with bimodal microstructures, it was confirmed that the degree of crystallinity governs the stiffness of the polymer. However, the energy dampening properties of the polymers benefit from the presence of the copolymer. A balance of stiffness and toughness can be obtained by altering the composition of the blends. For some blends, the presence of HMW homopolymer can dominate the tensile properties, showing little variation in the stiffness with increased addition of copolymer. It was also demonstrated that the testing conditions and thermal treatment of the polymer greatly influence the resulting elastic and energy dampening properties. Depending on the desired application, annealing these polymers (especially very low density copolymers) not only increases the crystallinity and stiffness, but also changes the frequency response of the dynamic mechanical properties.

Keywords: Polyethylene; Dynamic mechanical properties; Structure–property

1. Introduction

Commercially, there are numerous polyolefin resins available that have been tailored specifically for certain product applications and polymer processing operations. The applications range from piping, packaging, household and industrial containers to automotive, and are processed by extrusion, blown film, blow moulding and injection moulding processes, just to name a few. Many grades of resins are manufactured around the world and are commonly classified by their chemical composition, density, and melt index to identify their end-use application and processing operation [1].

For polyolefins, it is well known that both the molecular weight and comonomer distribution of a polymer play a vital role in determining their physical and processing properties. The microstructural features of these polymers include: the monomer and comonomer type, long chain branch length and distribution, comonomer content and comonomer distribution, molecular weight, and molecular weight distribution (MWD). All of these structural features can be traced back to the original production of the polymer [2].

The structural features of polyethylene are controlled during the polymerization and depend on the catalyst type and polymerization process. High-pressure processes using free radical initiators can produce only low density polyethylene (LDPE) that contains both short and long chain branches. Better microstructural control is possible with heterogeneous Ziegler–Natta or Phillips catalysts to produce linear high density polyethylene (HDPE) and copolymers of ethylene and α-olefins such as linear low density polyethylene (LLDPE). Currently, the polyolefin industry is also producing polyolefins with single-site catalyst technology to further control the polymer microstructure. These resins have narrow MWDs and uniform comonomer distributions [3] and belong to an entirely different class of polymeric materials.

* Corresponding author. Tel.: +1-519-888-4567x3436; fax: +1-519-888-6179.

E-mail address: jsoares@cape.uwaterloo.ca (J. Soares).

0032-3861/02/$ - see front matter
PII: S0032-3861(02)00703-6

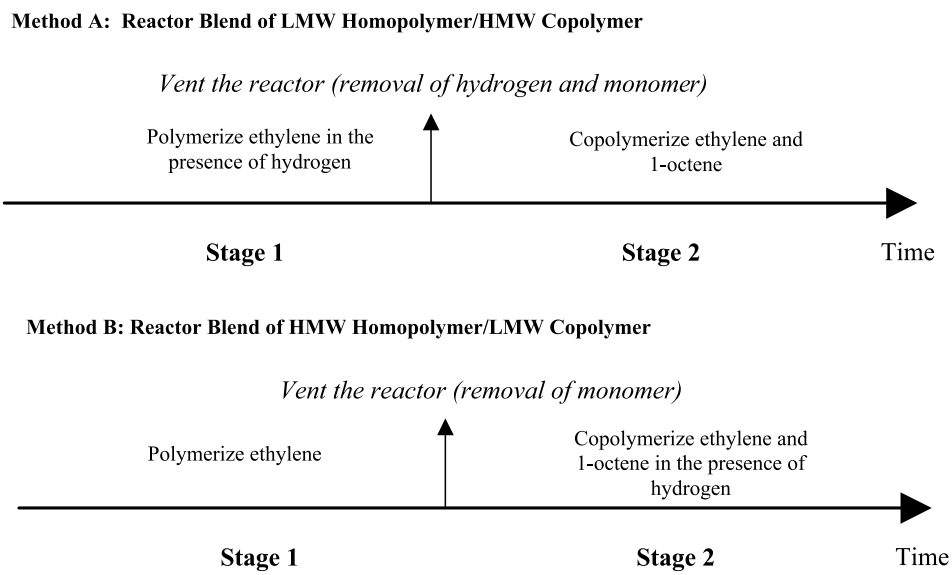

Fig. 1. Two-step polymerization methods.

However, with a single-site catalyst and single reactor process, polymers with unimodal structural distributions are usually obtained. It is difficult to tailor the properties of resins with unimodal structural distributions. If the MWD needs to be tuned, the entire distribution is shifted, resulting in a trade-off; one property is improved and another property is compromised [4]. Physical properties of the polymer such as stiffness and toughness are influenced by its molecular weight and degree of crystallinity. Increasing the molecular weight of a polymer decreases its degree of crystallinity [5,6]. Greater control over the crystalline density is often achieved by copolymerizing ethylene with α-olefin comonomers to increase the degree of short chain branching. Short chain branching reduces the crystalline density and lowers the polymer stiffness, but increases its toughness and optical clarity [7,8]. Even though high molecular weight (HMW) materials exhibit good toughness, they are inherently difficult to process because of their high melt viscosities. Processing polymers with high melt viscosities can be overcome with the use of processing aids but this solution is also costly.

To overcome the shortcoming of this property-processing relationship, a balance of properties can be achieved by the blending of polymers. One option is to melt-blend the polymers using an extruder or melt mixer. However, difficulties arise in obtaining well-dispersed morphologies at an attractive cost if the structural units differ greatly [9]. To tailor the polymer microstructure during polymerization, tandem or cascade type processes are often used to control the molecular weight and comonomer distribution of the polymer. A multiple staged process allows for the production of reactor blends (i.e. blends of polymers with different average properties directly produced in two or more reactors in series) containing the desired molecular components. Tailoring the microstructure of polyolefin resins through the use of bimodal structures, allows the control of the properties of each resin to fit the desired end-use properties and applications [4,10–12].

Given the interest in resins with bimodal structural distributions, our study was initiated to investigate and further develop the understanding of structure–property relationships of these resins. Of interest was the influence of the molecular weight and comonomer content of the individual polymer components and their contribution to the physical properties. Using a heterogeneous metallocene catalyst system, under the appropriate polymerization conditions, resins with controlled molecular weight and chemical composition distributions were synthesized. As an alternative to a tandem or cascade type process, a two-step polymerization method was carried out in a single reactor on a laboratory scale. Utilizing this two-step polymerization process, reactor blends of low molecular weight (LMW) homopolymer and HMW copolymer were produced that are similar to industrial resins with reverse comonomer distributions. For comparison, resins with conventional comonomer distributions were also synthesized, thus mimicking Ziegler–Natta LLDPE. These reactor blends consist of HMW homopolymer and LMW copolymer. For example, to synthesize a reactor blend of LMW homopolymer and HMW copolymer the method used is shown in Fig. 1a. In the first stage, ethylene was polymerized in the presence of a chain transfer agent such as hydrogen to produce LMW homopolymer. After venting the reactor to remove hydrogen, the second stage of the polymerization was carried out in the presence of 1-octene. Depending on the polymerization time and rate for each stage, reactor blends of polyethylene/poly(ethylene-*co*-1-octene) resulted. The homopolymer/copolymer ratios were manipulated by varying the polymerization time for each stage.

Fig. 1b shows the method to produce blends with conventional comonomer distributions. A blend of HMW homopolymer and LMW copolymer was produced by the

Table 1
Reaction conditions for the two-step polymerizations

Sample[a]	Stage	Temperature (°C)	Ethylene pressure (psig)	Hydrogen (ml)	1-Octene/ethylene ratio
1A	1st	70	250	150	–
1B	1st	70	250	150	–
	2nd	70	250	–	0.265
1C	1st	70	250	150	–
	2nd	70	250	–	0.265
1D	1st	70	250	150	–
	2nd	70	250	–	0.265
1E	1st	70	250	150	–
	2nd	70	250	–	0.265
1F	1st	70	250	–	0.265
3A	1st	60	250	0	0
3B	1st	60	250	0	0
	2nd	70	250	250	0.265
3C	1st	60	250	0	0
	2nd	70	250	250	0.265
3D	1st	70	250	250	0.265

'–' represents value not measured.
[a] Polymerization conditions: [Me_2Si(2-Me-4,5 BenzInd)$_2ZrCl_2$] = 1.25 μmol/l, support Al/Zr = 500, activator Al/support Al = 5.335.

addition of hydrogen and comonomer to the second copolymerization stage. Note that due to the difficulty in removing the unreacted comonomer from the reactor, only the copolymer could be produced in the second stage.

In this study, two sets of polyethylene/poly(ethylene-*co*-1-octene) resins were produced. The compositions of these blends range from LMW homopolymer to HMW copolymer and, vice versa, HMW homopolymer to LMW copolymer. The microstructure of each polymer was characterized for its molecular weight and short chain branching distribution. Physical property testing included uniaxial tensile testing under short-term loading conditions and the viscoelastic properties from dynamic mechanical analysis. Part II of this paper discusses the melt rheological properties from oscillatory shear measurements.

2. Experimental

As mentioned above, reactor blends covering a wide product range were synthesized. Using the two-step polymerization process, reactor blends of LMW homopolymer and HMW copolymer and blends of HMW homopolymer and LMW copolymer were prepared. The blends varied in composition from 100% homopolymer to 100% copolymer with mixtures ranging from 20 to 70%.

2.1. Sample production

Reactor blends of polyethylene homopolymer and poly(ethylene-*co*-1-octene) copolymer samples were produced with an in situ supported metallocene catalyst system [13,14]. This in situ system eliminates the need for a catalyst supporting stage by combining the catalyst preparation and polymerization in one-step. The resulting polymer has good particle morphology and high bulk density. These studies utilized *rac*-(dimethylsilylbis(methylbenzoindenyl)) zirconium dichloride [Me_2Si(2-Me-4,5 BenzInd)$_2ZrCl_2$] (Boulder Scientific, BSC 366), a silica support with a high weight percent of methylaluminoxane (provided by Witco), and triethylaluminum as an activator. Slurry polymerizations with *n*-hexane as a solvent were carried out in a 1 l semi-batch autoclave reactor (Pressure Product Industries, LC Series) operating between 60 and 70 °C and ethylene pressure of 250 psig.

The reaction conditions for each polymerization and stage are listed in Table 1. Both the comonomer and solvent were dried over molecular sieves and sparged with prepurified nitrogen. When required, hydrogen was added via a transfer syringe from a hydrogen bottle. Depending on the reactor blend required, the chain transfer agent was added prior to stage 1 or stage 2 polymerization. After stage 1, the reactor was depressurized and vented to the atmosphere. Prior to the second stage, 1-octene was added into the reactor via a transfer syringe. The initial concentration of 1-octene in the reactor was 0.425 mol/l or 21 mol% of 1-octene in the feed. The polymerization runs were carried out under similar conditions and limited in such a way to minimize the drift in comonomer composition. After the completion of each polymerization, acidified ethanol was injected into the reactor before depressurization. The polymer and solvent were washed with copious amounts of ethanol and then filtered and dried in an oven at 80 °C.

2.2. Microstructural characterization

The polymer samples were characterized for their MWDs using a Waters 150CV high temperature gel permeation chromatograph (GPC) and a Viscotek 150R

viscometer. The mobile phase used was 1,2,4 trichlorobenzene operating at 140 °C. The average molecular weights were determined using a universal calibration curve derived from narrow polystyrene standards.

Short chain branching distributions (SCBD) were determined by crystallization analysis fractionation (CRYSTAF) in 1,2,4 trichlorobenzene using a CRYSTAF 200 unit (Polymer Char, Spain). The samples were dissolved at 160 °C for 1 h and then cooled to 95 °C to begin the analysis. The sampling temperatures ranged from 95 to 30 °C at a cooling rate of 0.2 °C/min. 1-Octene comonomer compositions were determined by integrating the resulting CRYSTAF profiles while applying a calibration curve to relate the crystallization temperature and 1-octene composition [15]. This calibration curve was previously determined by ^{13}C NMR.

Melting endotherms were determined using a TA 2100 differential scanning calorimeter (DSC). The samples were heated from 35 to 200 °C at 10 °C/min, air cooled to 35 °C and then reheated from 35 to 200 °C at 10 °C/min. The melting point and degree of crystallinity of the polymer were estimated from the second pass. The degree of crystallinity was estimated by comparing the DSC melting enthalpy to that of a perfect polyethylene crystal ($\Delta H \approx 289$ J/g) [16].

2.3. Mechanical testing

2.3.1. Tensile testing

Tensile properties were determined according to ASTM D638 using an Instron 4465 materials tester. Dog-bone shaped samples (type V) were micro-injection moulded at 250 °C using an in-house melt mixing and moulding device. The samples were melted for 5 min and then injected under hand pressure into a heated mould. The mould and samples were then water-cooled. The samples were tested at a displacement rate of 25 mm/min and the grip-to-grip length was 3 cm. The sample yield and ultimate break strengths were determined from the force versus displacement curve during deformation of the sample. After testing, the increase in the gage length as compared to the original was used to determine the overall percent elongation.

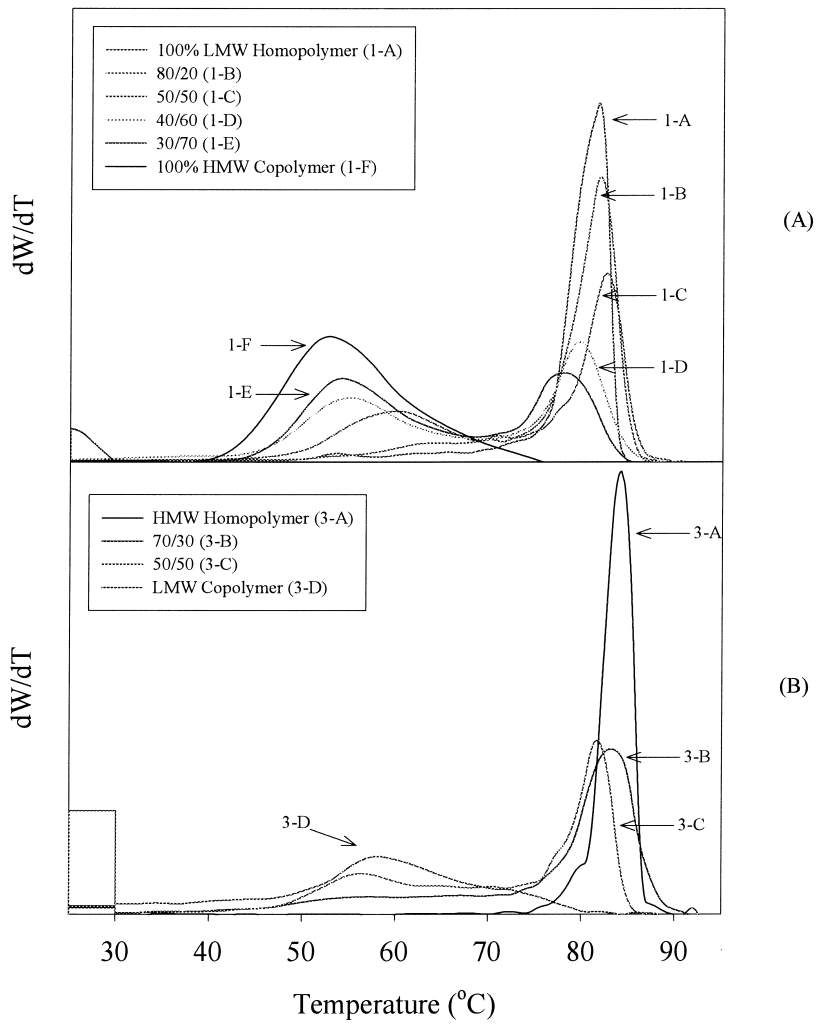

Fig. 2. Comonomer distributions of reactor blends.

2.3.2. Dynamic mechanical analysis

The dynamic mechanical properties of the polymer samples were measured by a Rheometrics DMTA V mechanical spectrometer. The samples were melt pressed at 200 °C into thin films and quenched in a water bath or air-cooled to room temperature. The films were then cut into rectangular specimens (25 mm × 10 mm × 0.1 to 0.2 mm). Storage (E') and loss (E'') moduli were measured in the tensile mode. Dynamic strains sweeps were carried out between 0.005 to 1.2% strain at 10 Hz and room temperature. Dynamic frequency sweeps were performed over the range of 0.01 to 100 Hz at room temperature and 0.05% strain. Dynamic temperature sweeps were carried out over a temperature range of −150 to 100 °C at a scanning rate of 3 °C/min, a frequency of 10 Hz and a strain of 0.05%.

3. Results and discussion

In this study, two sets of resins were produced. Each set contains a pure homopolymer, a pure copolymer and blends that increase in copolymer content. Set 1 are reactor blends of LMW homopolymer and HMW copolymer, similar to industrial resins with reverse comonomer distributions. The blends in Set 3 are the opposite in composition of Set 1 and are composed of HMW homopolymer and LMW copolymer. Table 1 shows the experimental details for the production of these resins. The homopolymer/copolymer ratio in the blend was achieved by monitoring the polymerization rate and the polymerization time for each stage.

Overall, the two-step polymerization method was successful in producing reactor blends in high yields for characterization and physical property testing. The discussion of the experimental results will be organized as follows:

Microstructural characterization

- Chemical composition distribution analysis by CRYSTAF - profile of the distribution of crystalline species, fractional estimation of homopolymer/copolymer amounts and comonomer content estimation.
- MWD analysis by GPC—number and weight average molecular weights, polydispersity index.

Physical property testing

- Melting characteristics as determined by DSC—melting point and degree of crystallinity estimates.
- Tensile properties (short term loading), yield stress, break stress and percent elongation.
- Dynamic mechanical properties—viscoelastic properties measured as elastic (E') and loss (E'') and tan delta (E''/E') responses with the effect of strain%, temperature and frequency.

3.1. Microstructural characterization

Two of the most important structural features of these resins are their short chain branching and MWD. The SCBD of the resins were determined by CRYSTAF. The resulting SCBD verified the presence and location of the copolymer fraction within the blended polymer. By comparing the SCBD of a pure homopolymer and pure copolymer, the location and amount of copolymer in the blend can be inferred. The MWDs were determined from GPC.

Fig. 2a and b compares the SCBDs of the two sets of resins. Set 1 includes two pure resins, a LMW homopolymer (1A) and HMW copolymer (1F) along with four reactor blends that increase in copolymer content (Samples 1B–1E). The pure homopolymer (1A) exhibits a narrow crystallization peak at 82.5 °C. Polymer crystallizing in this high temperature region will be considered to be homopolymer with very little or no comonomer in the polymer. The pure copolymer (1F) displays a very broad SCBD with a much lower crystallization temperature around 55 °C. Polymers that crystallize in this low temperature range have fairly high comonomer content around 4.0 mol%. The SCBD for this sample was quite broad, with crystallization temperatures between 50 and 70 °C. For a single-site catalyst, a sharp and narrow distribution was expected, but copolymers produced with in situ supported catalysts sometimes exhibit broad SCBDs [14]. This broadening may be due to the heterogeneity in the catalyst support sites. For these reactor blends, it is fairly easy to distinguish the LMW homopolymer and HMW copolymer, since the peaks and tails of each polymer population are fairly well separated. As shown, the copolymer peak increases for reactor blends 1B–1E, with the increasing fraction of copolymer. Also observed is the decrease in the height of the homopolymer peaks with the increasing fraction of copolymer. The height and area of these peaks are related to the weight fraction of the polymer present in each population. Using a calibration curve to relate the crystallization temperature with the 1-octene content of the copolymer (which was previously estimated by ^{13}C NMR) the comonomer content in mol% was estimated by integration of the SCBD. Table 2 shows for Set 1 that the comonomer content reaches a maximum of 4 mol% of 1-octene for the HMW copolymer (1F) and the 1-octene content increases with the fraction of copolymer present in the blend, as expected. The measured weight fractions of the homopolymer and copolymer present in the blends are also listed in Table 2. These fractions were estimated by integration of the CRYSTAF profiles for the regions deemed as homopolymer and copolymer.

Set 3 consists of reactor blends of HMW homopolymer and LMW copolymer. Set 3 has four resins: a pure HMW Homopolymer (3A), a pure LMW copolymer (3D), and reactor blends of 70/30 (3B) and 50/50 HMW homopolymer/LMW copolymer (3C). Fig. 2b shows the CRYSTAF profiles of the resins produced. A large homopolymer

Table 2
Microstructural properties of LMW homopolymer/HMW copolymer and HMW homopolymer/LMW copolymer blends

Sample[a]	$\bar{M}_N$[b] (g/mol)	$\bar{M}_W$[b] (g/mol)	$\bar{M}_W/\bar{M}_n$[b]	1-Octene content[c] (mol%)	Estimated homopolymer /copolymer fraction[d]	Melting peak[e] (°C)	Crystallinity[f] (≈density)[g] (%) (g/cm^3)
100% LMW homopolymer (1A)	17,150	157,500	9.2	0	100/0	133.8	78.8 (0.967)
80/20 (1B)	19,000	268,350	14.1	0.8	80/20	–	–
50/50 (1C)	23,300	318,400	13.7	1.5	57/43	126.0	60.0 (0.948)
40/60 (1D)	25,400	411,500	16.2	2.4	42/58	–	–
30/70 (1E)	44,250	458,150	10.5	2.9	32/68	124.0[e]	48.1 (0.932)
100% HMW copolymer (1F)	133,100	423,000	3.2	4.0	0/100	100.8	21.3 (0.881)
100% HMW homopolymer (3A)	238,450	542,750	2.3	0.0	100/0	130.7	65.5 (0.954)
70/30 (3B)	16,750	334,550	20.0	1.3	68/32	126.5	60.5 (0.948)
50/50 (3C)	17,350	272,800	15.7	2.1	51/49	125.0	58.2 (0.946)
100% LMW copolymer (3D)	21,950	84,250	3.8	5.9	0/100	107.1	41.9 (0.923)

'–' represents value not measured.

[a] Polymerization conditions: [Me_2Si(2-Me-4,5 BenzInd)$_2ZrCl_2$] = 1.25 μmol/l, support Al/Zr = 500, activator Al/support Al = 5.335, stage 1: polymerization temperature = 70 °C, ethylene pressure = 250 psig, 150 ml hydrogen. Stage 2: polymerization temperature = 70 °C, ethylene pressure = 250 psig, [1-octene] = 0.425 mol/l (52 ml).

[b] As determined from GPC analysis based on a universal calibration curve derived from narrow polystyrene standards. The molecular weight averages reported are based on replicate runs.

[c] As determined from an integrated CRYSTAF profile and 1-octene temperature–composition calibration curve [15].

[d] As determined from an integrated CRYSTAF profile with regions deemed as polyethylene homopolymer and poly(ethylene-*co*-1-octene) copolymer.

[e] As determined by DSC. Note that these samples exhibited very broad but unimodal melting distributions with the exception of sample 1E (25/75) which displayed a bimodal melting profile.

[f] Crystallinity estimates based on DSC melting enthalpy as compared to a perfect crystalline polyethylene ($\Delta H \approx 289$ J/g) [16].

[g] Approximate density range estimated from a % crystallinity versus density calibration curve from Kim et al. [26].

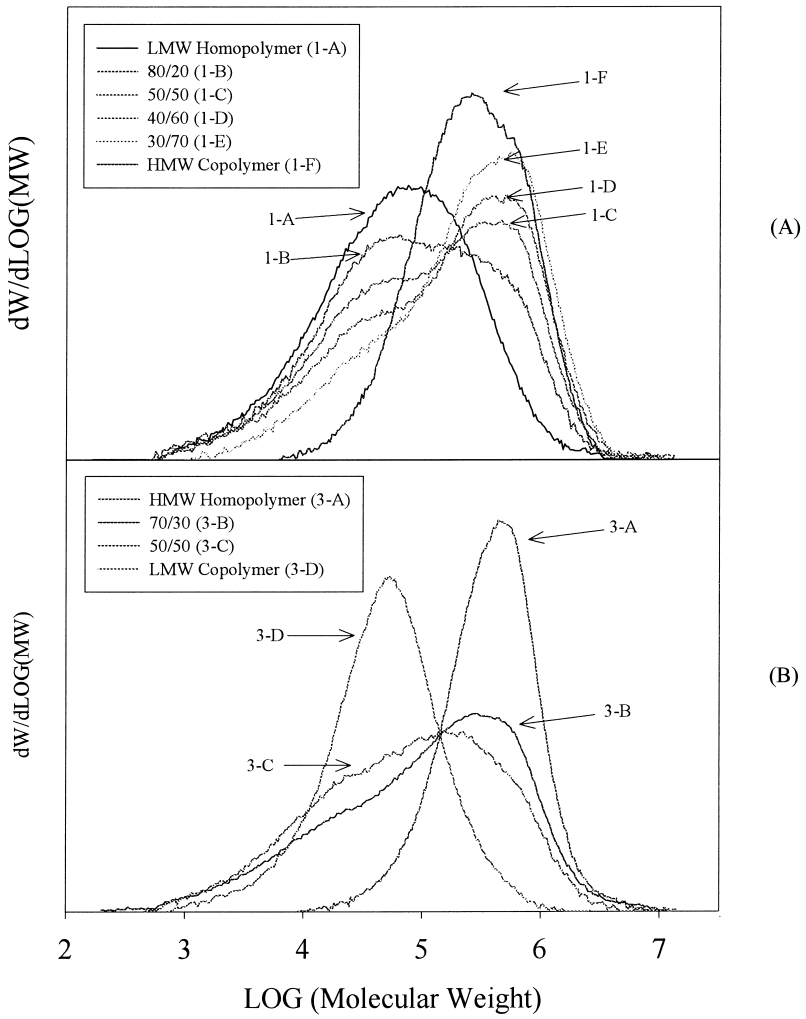

Fig. 3. MWDs of reactor blends.

fraction is present for reactor blends 3B and 3C. The profile of the LMW copolymer (3D) is also quite broad with the copolymer region extending from 50 to 80 °C. For these reactor blends, it can be seen that the profiles are not as well distinguished as in Set 1. Table 2 shows that the 1-octene content increases with the fraction of copolymer present in the blend. For the pure copolymer (3D), the comonomer incorporation was 6.0 mol% which is higher than the content of the HMW copolymer (1F) from Set 1. The polymerization conditions used to produce this copolymer fraction was similar to the second stage for Set 1, except for the fact that no hydrogen was added. The addition of hydrogen lowered the molecular weight of the polymer but also increased the incorporation of the comonomer. The CRYSTAF profile exemplifies this by showing very broad distributions for the copolymer blends. The broadening of the SCBD might be related to a change in the nature of the active sites or the increased solubility of the LMW copolymer.

From the CRYSTAF profiles, the measured crystallization temperatures, comonomer contents, and weight fractions verified that the reactor blends contain fractions of homopolymer and copolymer corresponding to the recipes of the two-step polymerizations used.

Fig. 3a and b shows the MWDs of the resins that were obtained from GPC analysis. The MWDs for Set 1 are shown in Fig. 3a and confirm that the copolymer (1F) has higher molecular weight than the homopolymer (1A). The separation between the number average molecular weights of these resins is approximately 8-fold, with the homopolymer having a number average MW of ≈17,000 and the copolymer ≈133,000. It has been reported by other researchers that the difference in the molecular weights must be around 10 times to achieve good separation [11,17]. The bimodal characteristics of the MWDs increase with increasing the fraction of HMW copolymer, thus demonstrating that the MWDs follow the recipe of the two-step polymerization method used. The polydispersity indices of these reactor blends were quite broad, varying from 10 to 16. It is noted that the polydispersity index of the pure LMW homopolymer was around nine and is much broader than expected from a single-site catalyst. It is possible that the hydrogen concentration in the reactor drifted during the polymerization. As a result, the hydrogen concentration will

Table 3
Tensile properties of reactor blends

Sample	Tensile strength at yield (kPa) (±777)[a]	Tensile strength at break (kPa) (±3650)[a]	Elongation at break (%) (±79.6)[a]
100% LMW homopolymer (1A)	29,200 (319)	20,800 (2963)	505 (112)
80/20 (1B)	22,700 (178)	23,800 (1966)	505 (74.0)
50/50 (1C)	16,000 (226)	18,900	440
40/60 (1D)	12,300 (331)	16,900 (3279)	376 (76.5)
30/70 (1E)	11,100 (554)	14,000 (2738)	362 (75.2)
100% HMW copolymer (1F)	7,440 (283)	16,300 (4,343)	468 (75.8)
100% HMW homopolymer (3A)	19,400 (367)	16,100 (1741)	195 (119)
70/30 (3B)	15,700 (1904)	15,300 (4550)	333 (239)
50/50 (3C)	16,600 (319)	27,900 (292)	705 (22.3)
100% LMW copolymer (3D)	9,480 (163)	17,200 (4506)	696 (140)

Testing conditions: ASTM D638 (type V), 3.175 mm thickness, grip to grip length 3 cm, displacement rate 25 mm/min, room temperature.
[a] Calculated standard deviations based on replicate testing.

decrease and higher molecular weight polymer will be produced as the polymerization proceeds [18]. Overall, for the resins in Set 1, the two-step polymerization method was successful in producing reactor blends of LMW homopolymer and HMW copolymer.

Fig. 3b shows the MWDs of the HMW homopolymer/LMW copolymer blends in Set 3. Good separation was achieved between the pure HMW homopolymer (3A) and pure LMW copolymer (3D). This separation resulted in reactor blends with very broad MWDs. Table 2 indicates that the molecular weight difference between the pure LMW copolymer and pure HMW homopolymer is about 10 times, with number average molecular weights of 22,000 and 240,000 g/mol, respectively. Both the homopolymer and copolymer exhibited fairly narrow MWDs with polydispersity indices of 2.3 and 3.8, respectively. The LMW copolymer (3D) exhibited less broadening of the MWD than that of LMW homopolymer (1F) in Set 1. It is possible that the combination of the comonomer and hydrogen together, created active sites that were more uniform and exhibited more single-site behavior. As a result of this large separation in the molecular weights, the reactor blends show very distinct and bimodal MWDs.

Overall, the GPC and CRYSTAF analyses have shown that the two-step polymerization method was successful in producing polyethylene/poly(ethylene-*co*-1-octene) resins with bimodal MWDs and bimodal SCBDs. Both the MWDs and SCBDs of these blends reflect the individual reactor conditions in which the polymer was produced.

3.2. Mechanical properties

The characterization of the resins produced by the two-step polymerizations has shown that their structures are well defined. Given these two sets of resins with bimodal structural distributions, structure–property relationships have been developed to better understand the influence of molecular weight, MWD, copolymer content and the molecular weight of the copolymer for these reactor blends. The contribution of each individual component, LMW and HMW homopolymer, LMW and HMW copolymer to the properties of the blends was observed. Commercially, there are numerous applications of these polymers and it is difficult to outline an optimum formulation unless a specific target grade was desired. The results from this study illustrate the general properties of these bimodal microstructures and could be used as a guideline for product development.

In this study, the influence of these bimodal resins on the solid-state and melt properties was examined. In the solid-state, both the tensile and dynamic mechanical properties of these bimodal resins were compared. The melt rheological characteristics were also measured but will be discussed in Part II of this paper.

3.2.1. Tensile testing

The tensile properties of the resins were measured under short-term loading conditions. The samples were stretched at a constant speed while the force and displacement were measured. From these deformation experiments, the yield and failure behavior up to high strain were used to estimate the tensile stresses at yield and at break. From the change in gage length of the sample, the percentage elongation at break was also calculated. The measured values for the two sets of resins are listed in Table 3 and compared in Figs. 4 and 5. In general, most of the samples exhibited localized yielding and cold drawing that is characteristic to semi-crystalline polymers. Figs. 6 and 7 compare the initial yielding behavior of the resins. It was found that the yield stress measurements were the most repeatable. The repeatability of the measurement of the yield stress was quite low when compared to the error associated with the tensile stress at break and percentage elongation at break. These errors may be linked to the difficulties encountered in the preparation of sample bars that were free from defects.

Fig. 4 compares the tensile stresses at yield for the blends of LMW homopolymer and HMW copolymer in Set 1. The tensile stress at yield was much higher for the LMW homopolymer (1A) than the HMW copolymer (1F). For these reactor blends, it can be clearly seen that yield stress

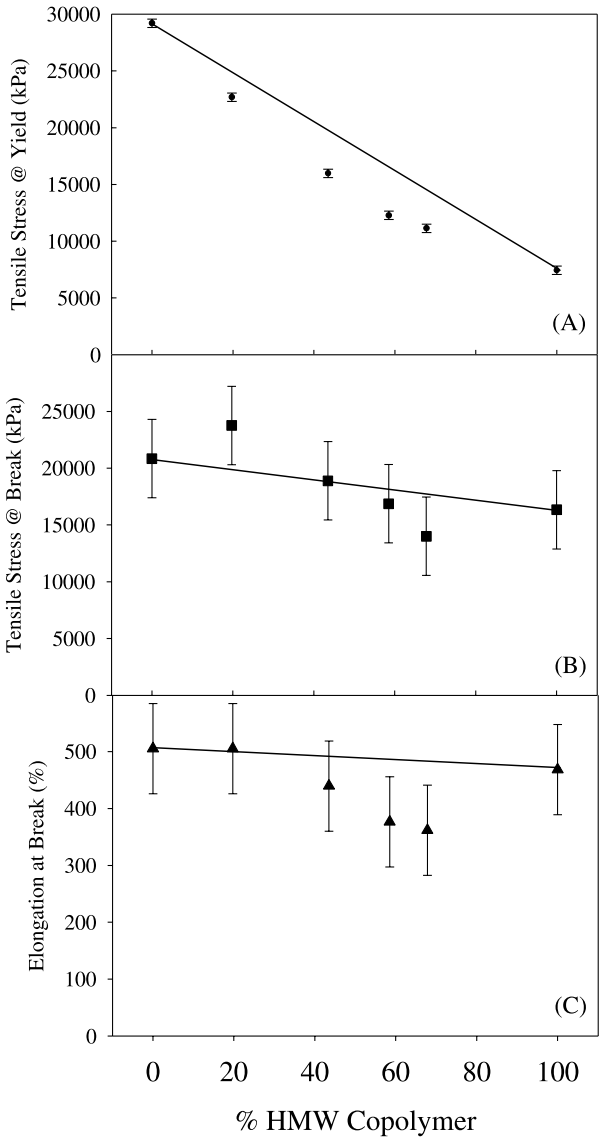

Fig. 4. Set 1: comparison of tensile properties of reactor blends.

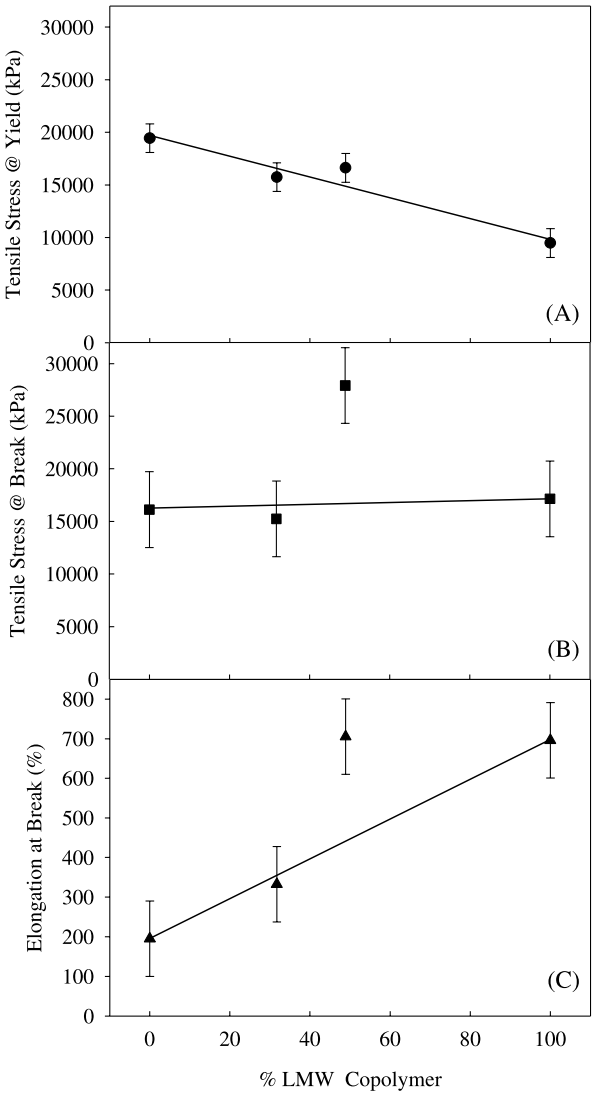

Fig. 5. Set 3: comparison of tensile properties of reactor blends.

decreases with increasing percentage of HMW copolymer. The results are quite consistent since the yield stresses decrease in an almost linear fashion. The trend observed should reflect the decrease in crystallinity of the polymer with the addition of the lower density material. The DSC measurements of the melting points and degree of crystallinity for these resins are listed in Table 2. As expected, the peak melting point of the pure homopolymer was the highest with a value of approximately 134 °C. Corresponding to the high melting point of the homopolymer, a high degree of crystallinity of 79% was estimated. On the other hand, the pure copolymer had the lowest melting point at 101 °C with a low degree of crystallinity of 21%. Both the melting point and degree of crystallinity decrease with increasing fraction of copolymer. The blends have values that are between that of the pure homopolymer and pure copolymer. Cho et al. have reported that blends of HDPE/LLDPE with similar molecular weights can cocrystallize with each other to result in blended properties closely following the rule of additivity [19]. Similarly, for these blends, it would be predicted that the yield stress would decrease linearly with increasing fraction of copolymer. However, a slight negative deviation was observed, since the yield stresses of the blends are slightly lower than predicted. Fig. 4b and c show the polymer deformation behavior at high strains. Increases in the fraction of HMW copolymer in the blends results in decreasing break strength and elongation at break. This may indicate that the LMW homopolymer and HMW copolymer do not cocrystallize efficiently resulting in a dispersed morphology. For these blends, it is not unreasonable that the crystallization behavior would be altered by the presence of different structural units. For the resins in Set 1, the molecular weights and comonomer contents of the individual components of these blends are quite distinct and the resulting crystal structure may not be as regular or intermixed as one would expect.

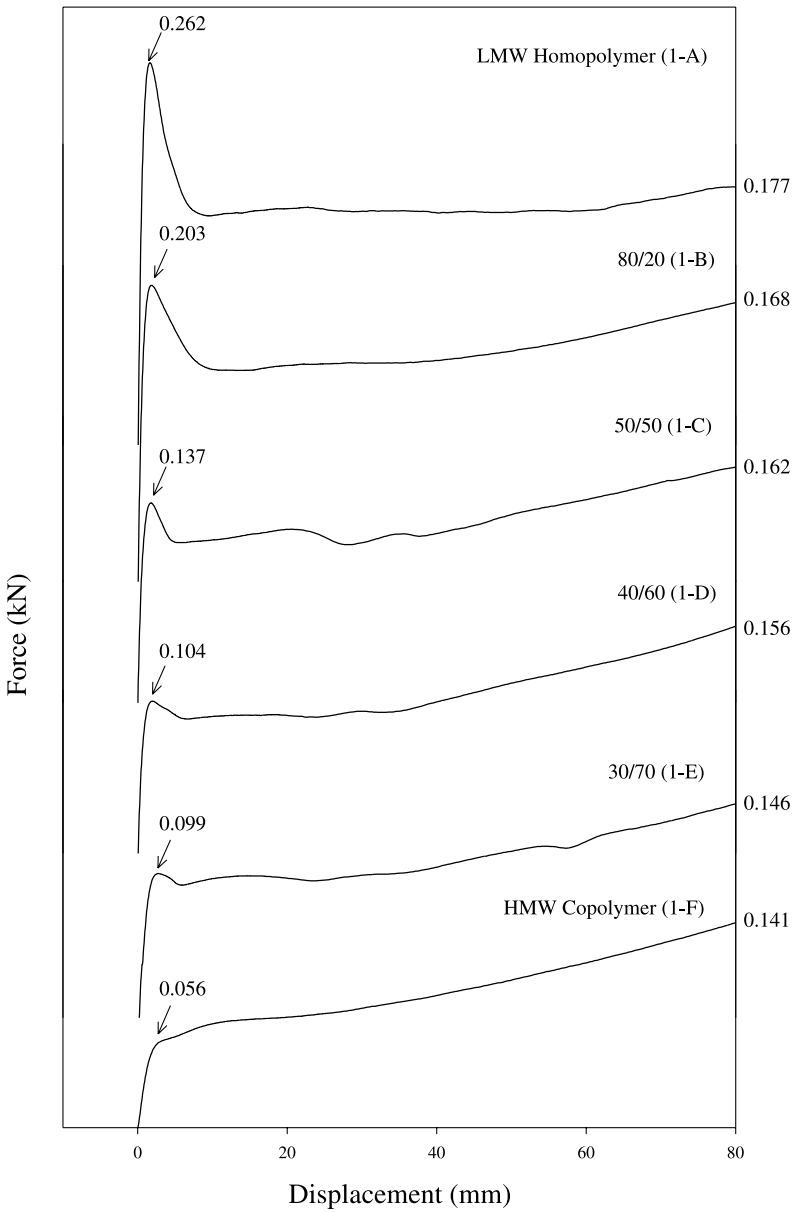

Conditions: room temperature, 25 mm/min, grip-to-grip length 3 cm
* Force values shown at yield and break.

Fig. 6. Set 1: comparison of initial tensile yielding behavior.

For Set 3, the composition of the blends (HMW homopolymer/LMW copolymer) is reverse to that of Set 1 (LMW homopolymer/HMW copolymer). Despite the differences in composition, Fig. 5a shows that the tensile stress at yield decreases with increasing LMW copolymer. However, it is noted that the tensile stresses at yield for sample 3B (70/30) and sample 3C (50/50) were very similar. Their degrees of crystallinity are also very similar (Table 2). Note that the degree of crystallinity for the HMW homopolymer (3A) is lower than that of the LMW homopolymer (1A) due to its HMW and narrower MWD which slows the crystallization process. The low degree of crystallinity also resulted in an unusually low estimate of the crystalline density for this high-density sample. However, despite the large fraction of copolymer, the HMW homopolymer seems to dominate the crystallization process, resulting in a degree of crystallinity that is similar for these blends. Fig. 5b and c compares the high strain tensile properties of these resins. As shown, the HMW homopolymer had very poor elongational properties. This poor performance may be attributed to testing errors (due to defects in the sample bars), but, it might also be possible that the HMW chains cannot disentangle within the crystallites and brittle fracture occurs.

Figs. 6 and 7 compare the initial deformation behavior for the two sets of resins. It was observed that broadening of

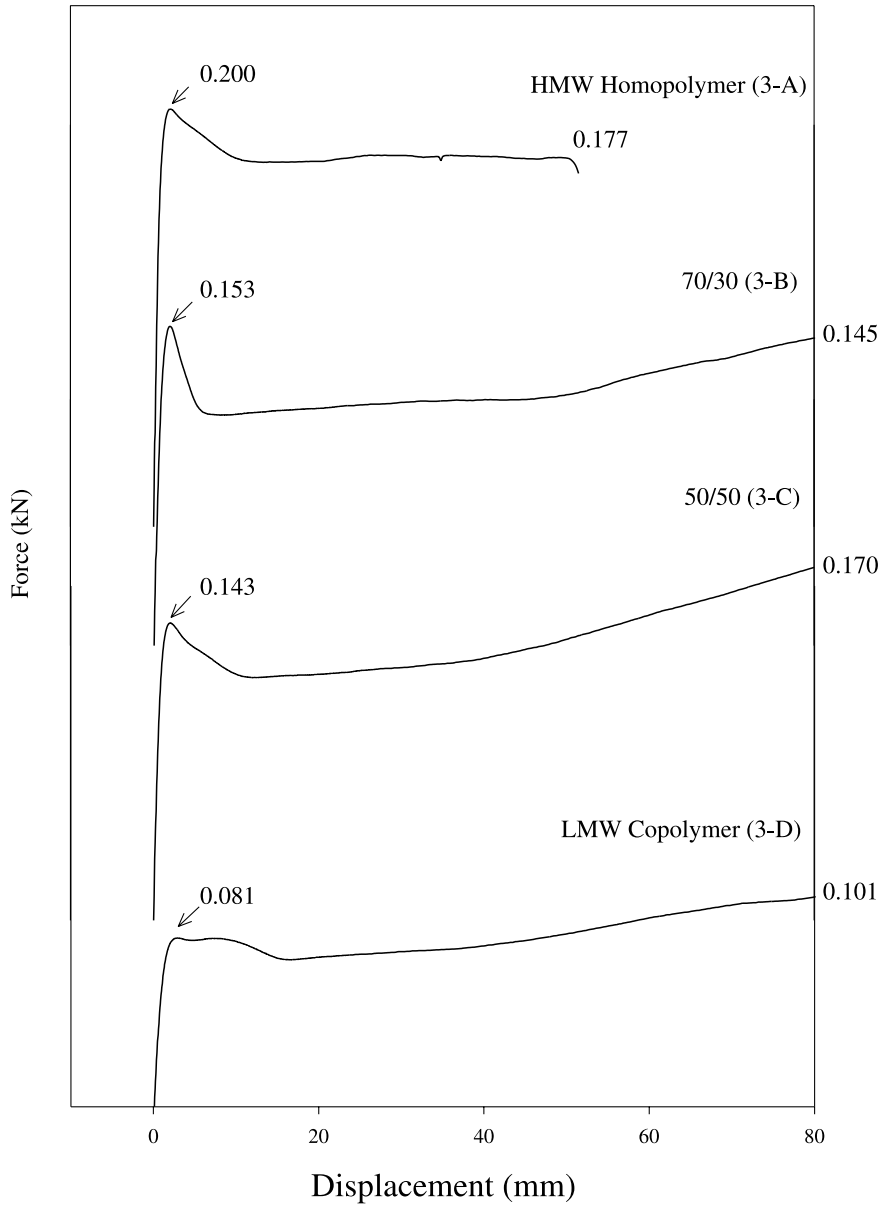

Conditions: room temperature, 25 mm/min, grip-to-grip length 3 cm
* Force values shown at yield and break.

Fig. 7. Set 3: comparison of initial tensile yielding behaviour.

the yielding zone occurs with increasing percentage of copolymer in the blend. For blends with greater than 50% copolymer, a broad yielding region was observed that could be classified as a double yield point. This double yield behavior has also been observed by others for polyethylene copolymers [8,20–22]. Bensason et al. reported that, with a decrease in density, the yield maximum broadens up to a point where it becomes indistinguishable and no yield maximum is observed [8]. Similarly for these samples, it appears that the yielding region broadens with decreasing degree of crystallinity or increasing comonomer content. Given the bimodal nature of these SCBD, increasing the proportion of higher crystalline homopolymer results in a narrower yield maximum except for the pure HMW homopolymer (3A) in Set 3. This sample should exhibit a narrower yield zone when compared to the reactor blends (3B, 3C). However, this was not the case. This sample has very HMW. Comparing this HMW homopolymer to the LMW homopolymer (sample 1A), the overall crystallinity for this sample is lower (66%) than that of the LMW homopolymer (1A) (79%). The HMW homopolymer may produce thinner crystallites than the LMW homopolymer.

Contrasting Sets 1 and 3, it is possible to compare the effects of molecular weight and degree of crystallinity on the tensile properties of these polymers. Fig. 8 shows an overlay of the tensile stresses at yield and the degrees of

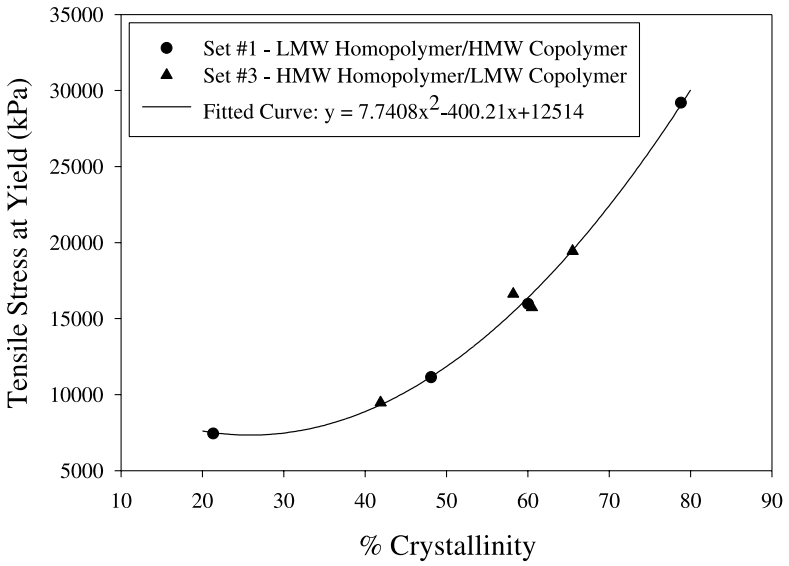

Fig. 8. Effects of blend composition and degree of crystallinity on tensile yield.

crystallinity for Sets 1 and 3. Despite the fact that Sets 1 and 3 have very different microstructures with varying compositions, it is shown that the data points overlap. Regardless of the microstructure, the degree of crystallinity seems to be the governing factor influencing the initial yield stress. Thus, it is inferred that the stiffness of polyethylene mostly depends on the achievable degree of crystallinity by its microstructure. This finding has also been evidenced by

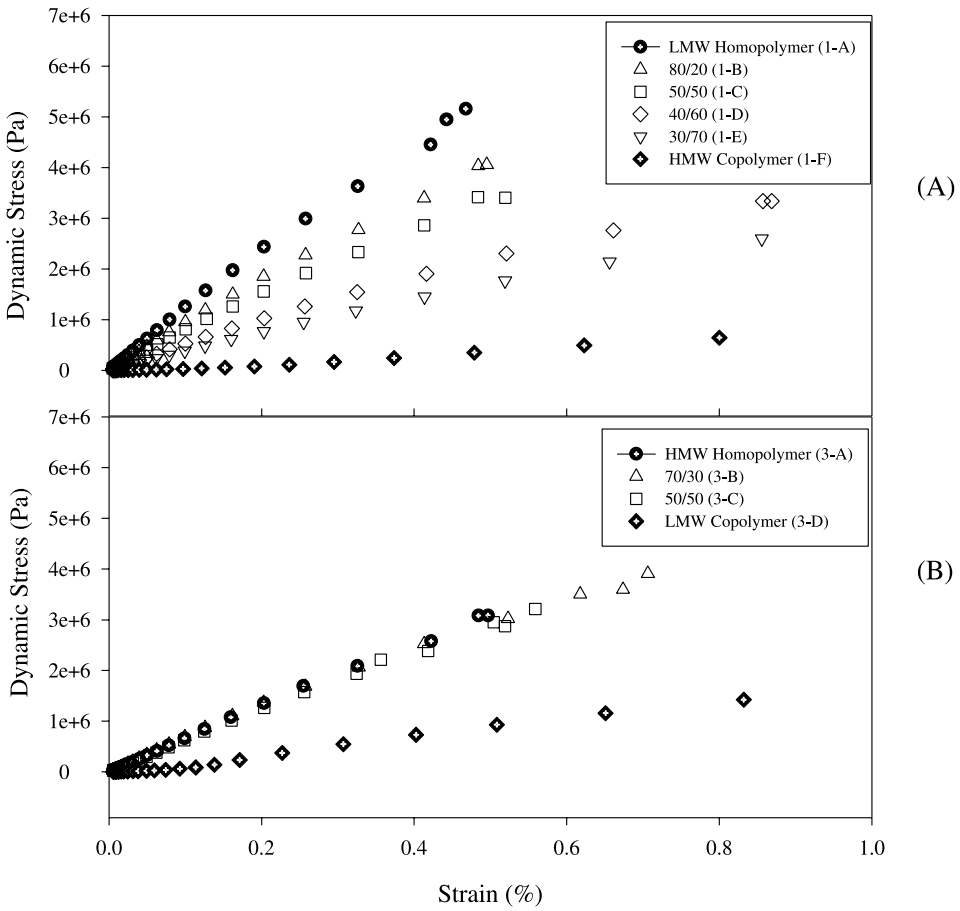

Conditions: Strain sweep,10 Hz, room temperature

Fig. 9. Dynamic stress–strain comparison of reactor blends.

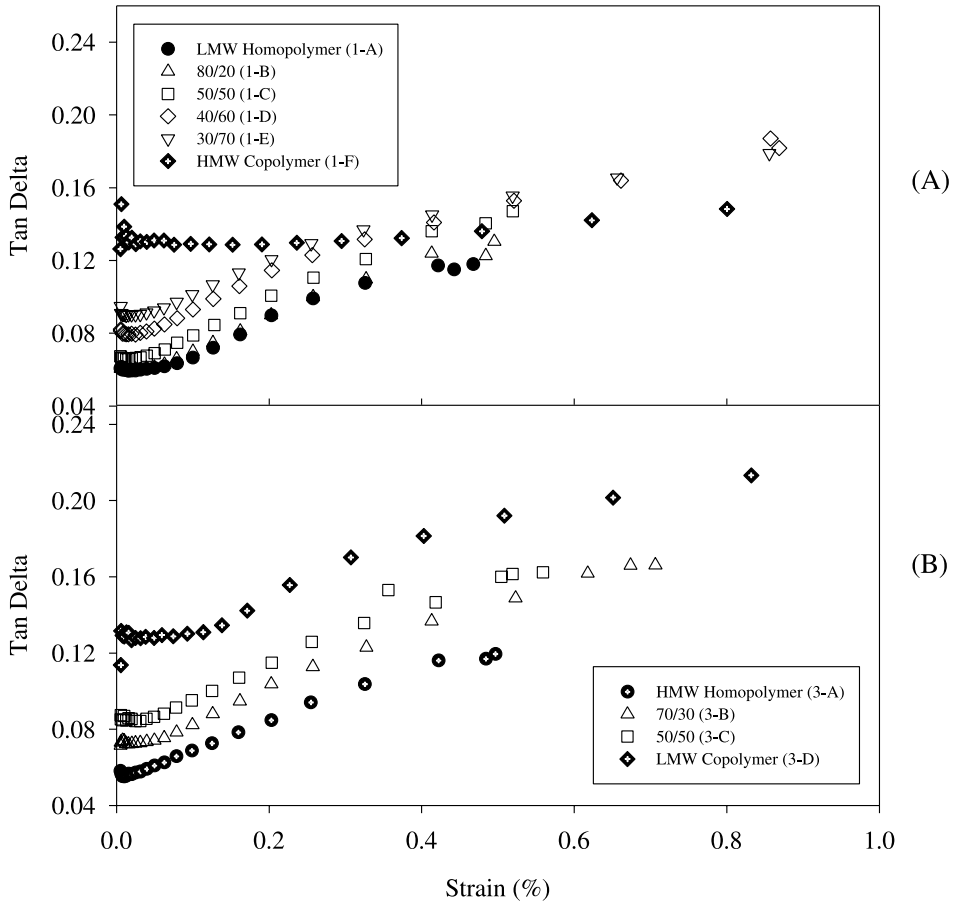

Conditions: Strain sweep,10 Hz, room temperature

Fig. 10. Energy dampening comparison of reactor blends under dynamic strain.

Simanke et al. for polyethylene copolymers with varying branch lengths [20] and by Grahm et al. for polyethylene with different molecular weights [21].

Overall, it can be inferred from these results that the tensile stress at yield decreases with decreasing degree of crystallinity of the polymer. The degree of crystallinity of the polymer can be lowered by the incorporation of comonomer or reactor blending of copolymers. Depending on the blend composition, different structural units may not form uniform crystal structures as evidenced by the negative deviations from linearity of the tensile properties.

3.2.2. Dynamic mechanical properties

In the following discussion, the dynamic mechanical properties of the resins will be compared to the tensile properties measured above. A dynamic stress–strain sweep is generally used to determine the strain range required for the test to remain within the viscoelastic region of the polymer. For these polymers, a strain level of 0.05% was found to be adequate. Fig. 9a compares the dynamic stress–strain behavior of the LMW homopolymer/HMW copolymer blends. Strains greater than 1% were not achievable due to the limitations of the analysis equipment. The deformation behavior of these resins was quite clear. The LMW homopolymer (1A) requires much higher dynamic stresses to achieve the desired % strain than the HMW copolymer (1F). The slope of the dynamic stress–strain curve decreases with increasing the fraction of copolymer in the blend (samples 1B–1E). As shown, the stiffness of the HMW copolymer can be enhanced with the addition of a small fraction of LMW homopolymer (compare samples 1F and 1E).

Different stress–strain behavior was observed for the blends of HMW homopolymer and LMW copolymer (Set 3). Fig. 9b shows little difference between the HMW homopolymer and the blends with 30 and 50% copolymer (3B, 3C). Contrasting these with the LMW copolymer (3D), the copolymer is much softer since it requires less stress to achieve the desired strain. These results compare well with those from the tensile testing, confirming that the HMW homopolymer tends to dominate the initial yielding behavior. The stiffness of these polymers seems to be dominated by the presence of very long molecules that are unable to relax and disentangle.

Fig. 10a shows that the energy dampening can be influenced by the fraction of LMW homopolymer for Set 1.

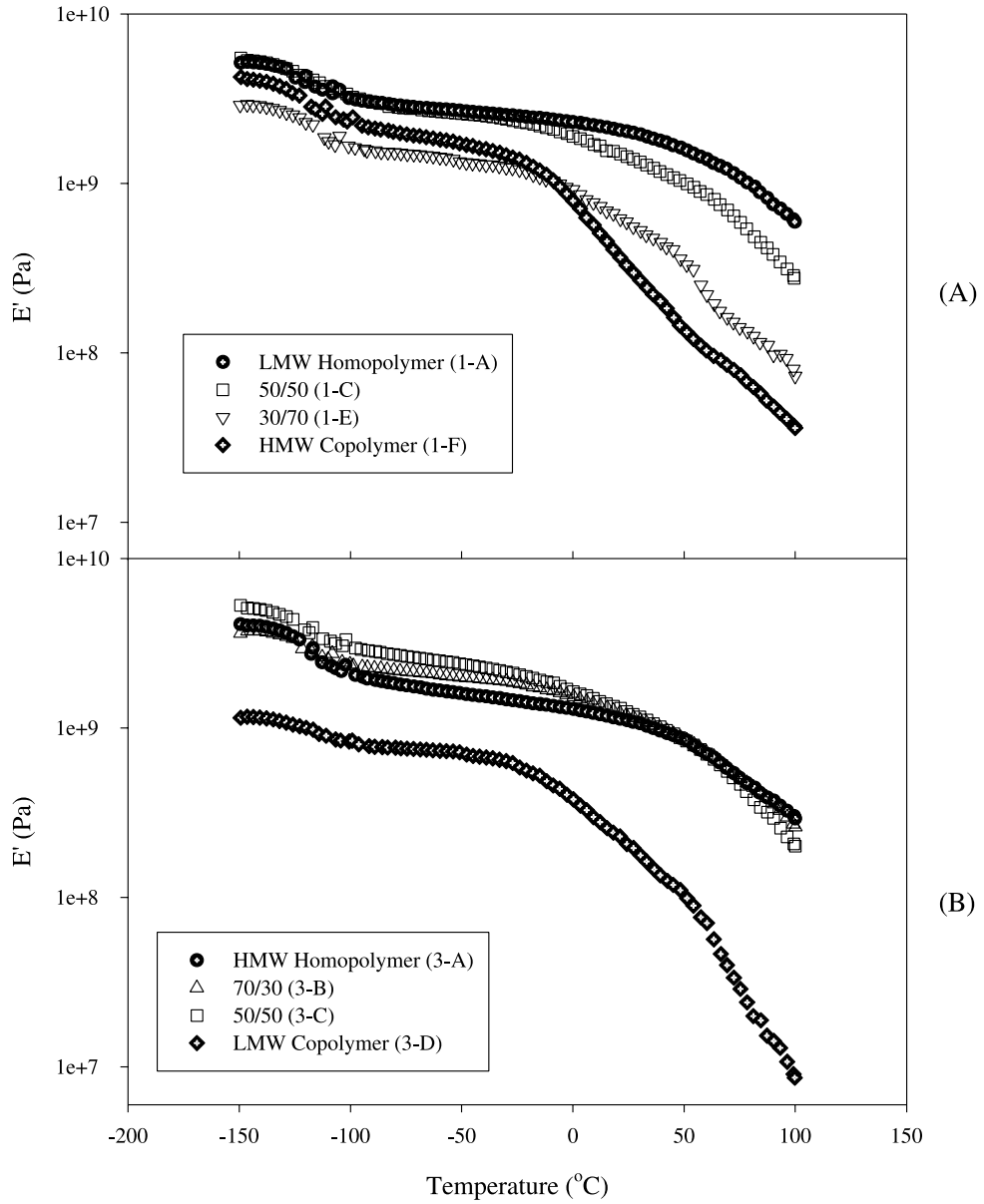

Conditions: Temperature sweep, 3 °C/min, 10 Hz, 0.05 % strain

Fig. 11. Effect of temperature on storage modulus of reactor blends.

At low percent strains (up to 0.05% in the linear viscoelastic region), the tan delta of the HMW copolymer (1F) is the highest. The tan delta decreases with decreasing percentage of copolymer, with the LMW homopolymer reaching the lowest value. It is consistent that the tan delta would decrease as the degree of crystallinity of the polymer increases because of the dissipation of energy into the amorphous regions. Increasing the strain beyond the linear viscoelastic region, the homopolymer's ability to dampen energy also increases. With increasing strain, the tan delta of the reactor blends eventually surpasses the tan delta of the HMW copolymer. The data for the LMW homopolymers (1A) and samples (1B, 1C) end abruptly at ≈0.5% strain due to the stress limitation of the testing instrument. In general, the energy dampening behavior of the blends benefits from the presence of LMW homopolymer at high strains. The enhancement of the tan delta is probably related to the strain hardening behavior of the sample once irreversible deformation occurs. Fig. 10b compares the tan delta versus %strain for Set 3. Similar to the behavior found for Set 1 at low strains, the LMW copolymer shows the highest energy dampening and decreases with increasing the fraction of HMW homopolymer. However, at high strains, the LMW copolymer (3D) maintained a higher tan delta than the HMW homopolymer (3A) and the blends (3B, 3C). In the discussion above, it was speculated that the elastic properties were dominated by the HMW homopolymer. From results shown in Fig. 10, it can be inferred

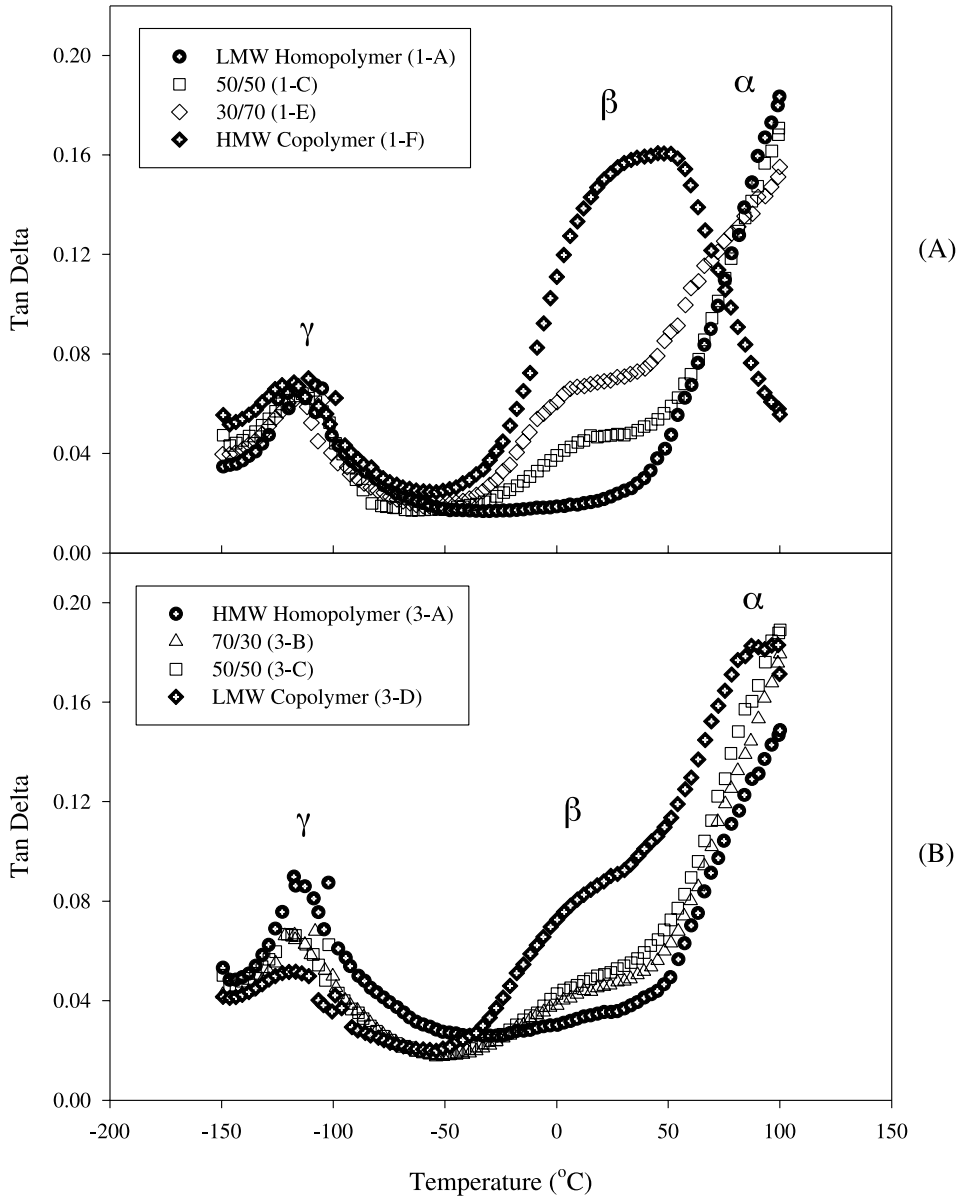

Fig. 12. Effect of temperature on the tan delta of reactor blends.

that the loss properties are highly influenced by the LMW copolymer.

Figs. 11 and 12 compare the effect of temperature on the dynamic mechanical properties for Sets 1 and 3. Fig. 11a and b shows that the storage modulus (E') decreases with increasing temperature for the resins. This behavior is typical of polymeric materials since the chain movement and relaxation times of the polymer are reduced at lower temperatures [23]. Above room temperature, the storage modulus decreases with increasing fraction of copolymer as expected. At and above room temperature, the storage moduli of these resins are consistent with the stress–strain results.

Fig. 12 shows the effect of temperature on the tan delta responses. For the temperature range studied, the samples exhibited the characteristic γ, β and α transitions for the loss modulus and tan delta. Although there is much debate on the existence and nature of these transitions, it is believed that they are linked to the motions of the amorphous and crystalline portions of the polyethylene chains [8,23–25]. Examining the tan delta behavior (Fig. 12a and b), the γ transition is often associated with the rotation of four carbon chain segments (Schatzki-crankshaft mechanism) and was observed around −120 °C [27]. The β-transition, that is often associated with the glass transition temperature of the amorphous polymer is due to the motion of the branched segments of the chains and occurred between −25 °C and room temperature [8,25]. Lastly, the α transition was also

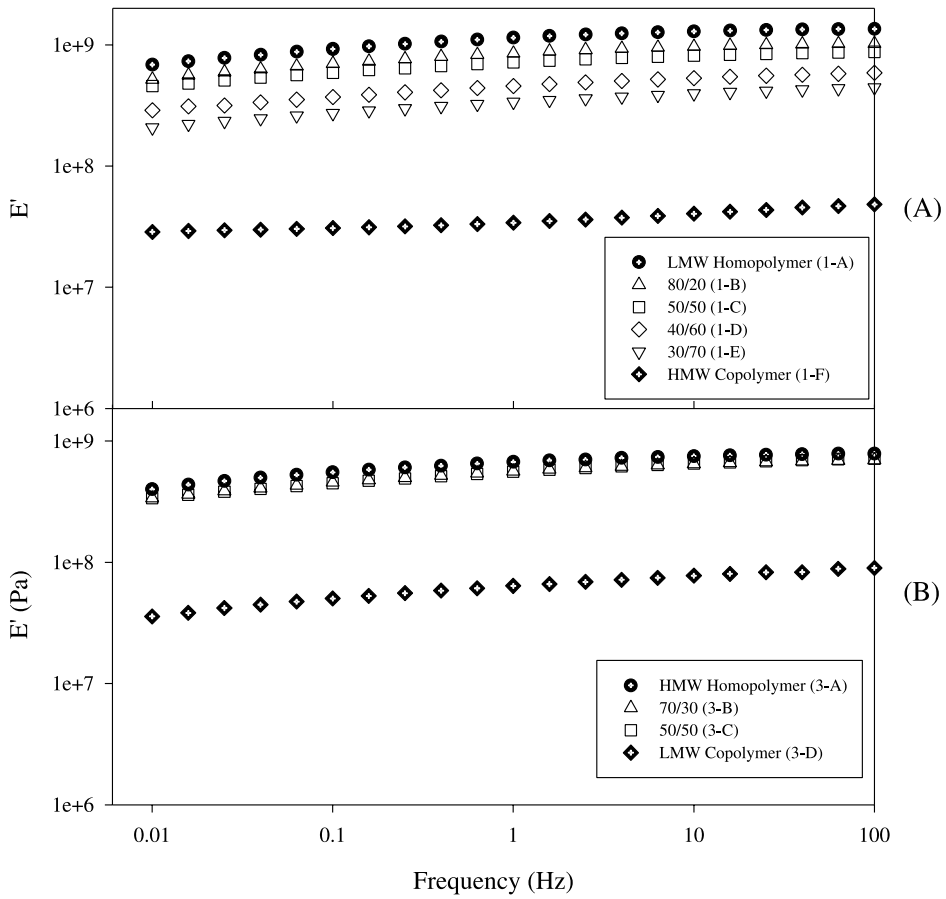

Conditions: Frequency sweep, room temperature, 0.05 % strain

Fig. 13. Effect of frequency on the storage modulus of reactor blends.

observed above 50 °C and this is generally attributed to the gradual motion of main chain units within the crystallites before the onset of melting. Comparing the tan delta response during γ-transition for both Sets 1 and 3, the tan delta values reached a maximum value at approximately −125 °C. For Set 3, it appears that the magnitude of this transition depends on the fraction of the HMW homopolymer: the pure HMW homopolymer exhibits the largest transition and the pure LMW copolymer the smallest. However, for Set 1, no discernible differences between the transition of the LMW homopolymer and HMW copolymer were observed. Therefore, it is difficult to pinpoint the influence of the microstructure on the nature of this transition. In the region of the β-transition, the effect of the fraction of copolymer is quite prominent. In both sets, the tan delta response increases with increasing copolymer fraction. Both homopolymers (samples 1A and 3A) show similar tan delta in this region. After the β-transition, the α-transition occurs as main chain motion between the crystallites begins. This α-transition occurs above room temperature and depends on the polymer composition. The earliest transition was displayed by the LMW copolymer and blends (3D, 3C, 3B or 1E, 1C) and the latest by the pure homopolymers (samples 1A and 3A), as expected. However, the HMW copolymer's (1F) alpha transition was not readily apparent. Mandelkern has deduced that the α transition mostly depends on the crystallite thickness, irrespective of molecular weight, branching type and concentration, and level of crystallinity [28]. This HMW copolymer sample had the lowest level of crystallinity and would probably lead to thinner crystallite lamellae when compared to the others resins in this study.

Frequency sweeps were performed at room temperature to verify the frequency dependence of the dynamic mechanical behavior. For the LMW homopolymer/HMW homopolymer blends, the stiffness (elastic modulus) of the polymer increases with increasing frequency (Fig. 13a and b). This behavior is typical since the polymer chains appear stiffer due to the reduced relaxation time. For these blends, the storage moduli decrease with increasing fraction of copolymer, thus reconfirming the observations from the tensile testing and other dynamic mechanical measurements.

Fig. 13b shows the dependence of the storage modulus with frequency for the HMW homopolymer/LMW copolymer blends (Set 3). As shown, the HMW homopolymer and the blends exhibit similar high moduli. These results are consistent in that the HMW homopolymer dominates the

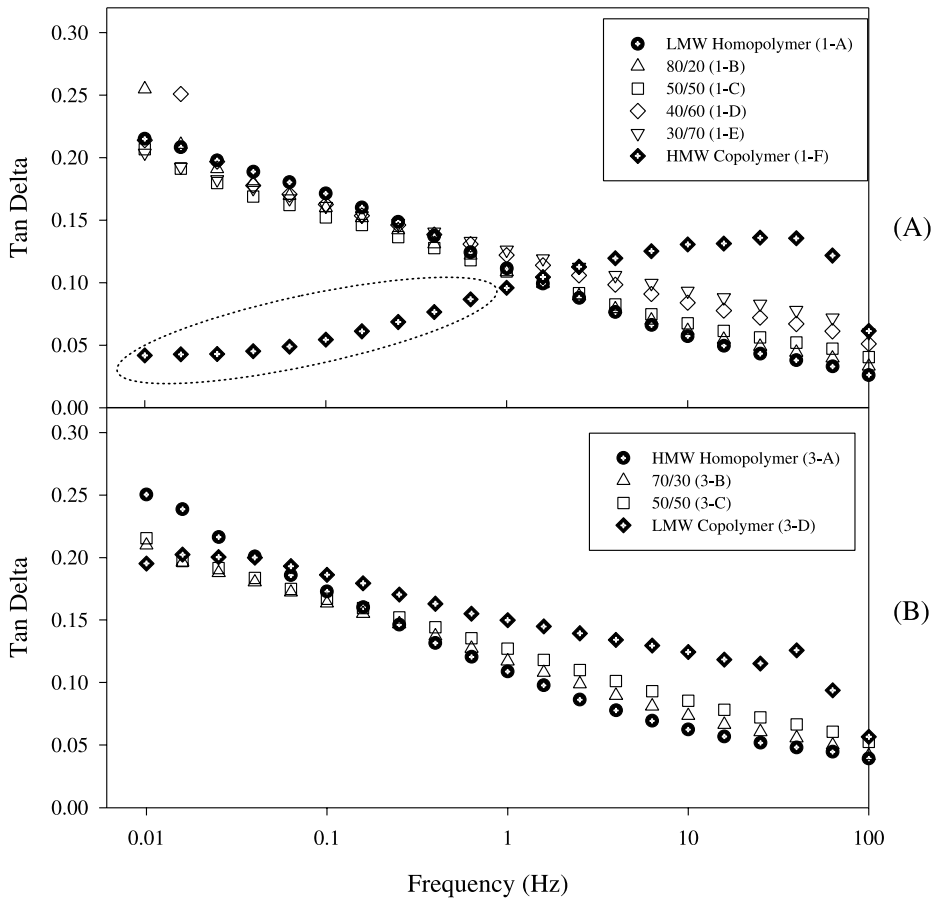

Conditions: Frequency sweep, room temperature, 0.05 % strain

Fig. 14. Effect of frequency on the energy dampening of reactor blends.

stiffness of the blends, as was also observed from other measurements discussed above.

Fig. 14a and b examines the frequency dependency of the tan delta (E''/E') responses for the resins. The tan delta responses of the samples decrease with increasing frequency of the test, except for sample 1F. The change in tan delta with frequency corresponds to a larger decrease in the loss response (E'') as compared to the increase in elastic response (E'). As the frequency of the test increases, the relaxation of the chains become faster lessening the loss response.

The reduction in tan delta varied depending on the blend composition. At frequencies above 2 Hz, the samples with higher fraction of HMW copolymer also have higher tan delta, showing that HMW copolymer dampens energy more efficiently than the LMW homopolymer. However, the dampening behavior of the HMW copolymer (1F) shows a different dependency on the frequency of the test. At frequencies below 2 Hz, the tan delta of the HMW copolymer is much lower than those of the other samples. Throughout the entire frequency range tested, the tan delta response of this copolymer increases, instead of decreasing, with increasing frequency of the test.

The low frequency behavior for this HMW copolymer was unexpected. Given the low density of this copolymer (0.881 g/cm^3), it probably possesses a disordered crystalline structure. Bensason et al. observed that elastomers and plastomers with very low densities (less than 0.905 g/cm^3) form mixtures of bundle-like and lamellar structures [8]. It is possible that the low frequency behavior observed here is the response of a copolymer with bundle-like crystals with ill-defined lamellar structure. The temperature sweep (Fig. 13a) of this HMW copolymer (1F) did not exhibit a distinct α-transition. Instead of an increase in tan delta, a sharp drop in tan delta was observed around 50 °C. Due to the low degree of crystallinity of this sample, above this temperature, the polymer chains behaved very liquid-like as shown by the sharp decrease in E' (Fig. 11a) and tan delta (Fig. 12a). The unusual frequency behavior observed for the copolymer (Fig. 14a) may be explained as the time-temperature equivalence of its transitional behavior, since the dynamic responses from oscillatory measurements depend on the frequency and temperature of the test [23].

Fig. 14b shows frequency dependence of the tan delta response for Set 3. As expected, the tan delta decreases with increasing frequency of the test, due to the apparent increase in stiffness of the material. Again in the low frequency range, there is little difference in the energy dampening until 0.1 Hz where the tan delta responses of the samples diverge,

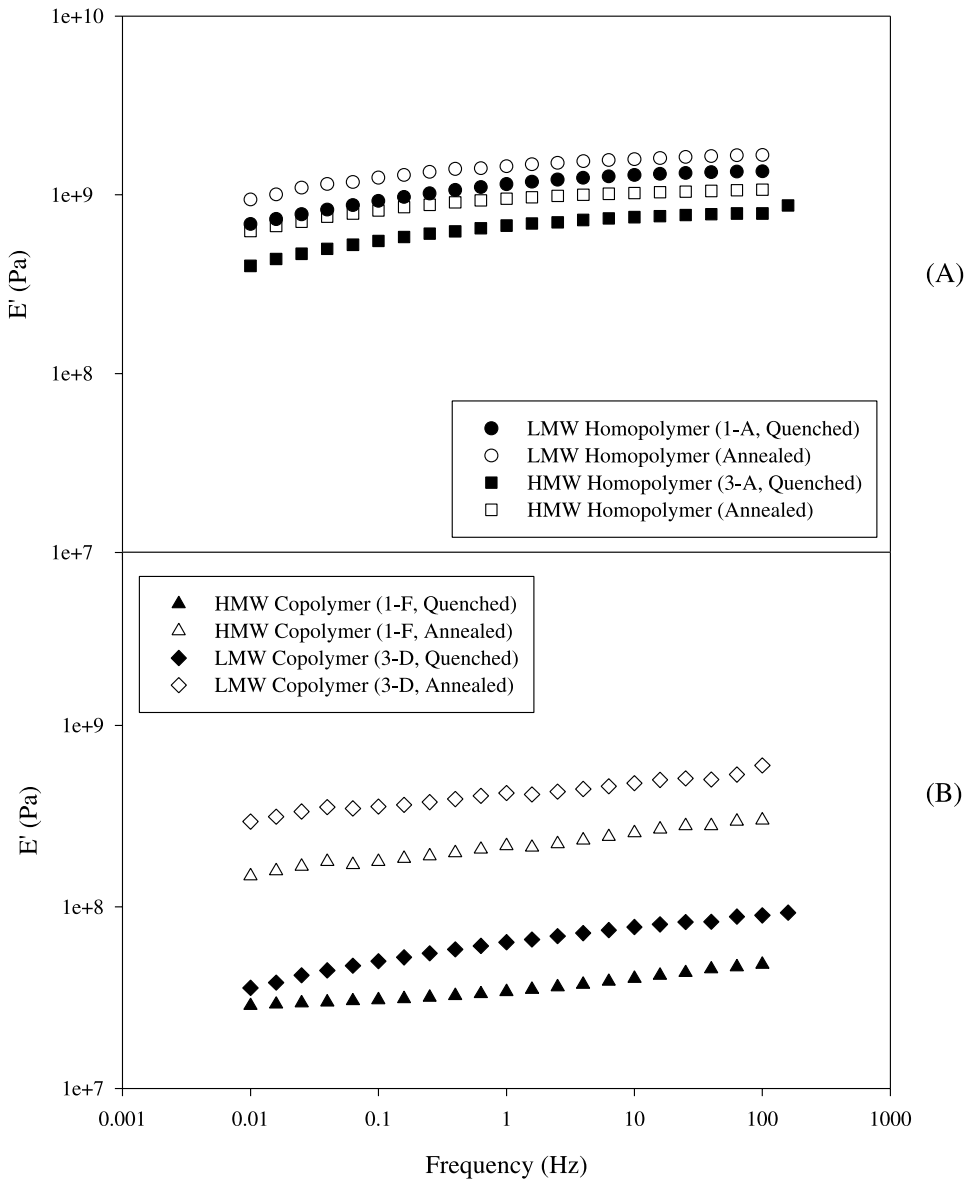

Fig. 15. Comparison of storage moduli between quenched and annealed polymers.

thus demonstrating the ability of the copolymer to absorb energy. However, it is noted that the stiffness of these materials was quite high. The dominance of the HMW material maintains the stiffness but the copolymer improves the energy dampening behavior.

To examine the effect of thermal history on the dynamic mechanical properties of the pure homopolymers and copolymers, quenched (water-cooled) and annealed (air-cooled) samples were also compared. Slower crystallization (slow cooling) allows for the formation of larger and more perfect crystals to increase the degree of crystallinity of the polymer. Fig. 15 shows that the storage modulus increases for both the homopolymer and copolymer after annealing, regardless of their molecular weight. For the pure homopolymers, the increase in E' was approximately 20–40% for the LMW homopolymer (1A) and 35–55% for the HMW homopolymer (3A). On the other hand, the pure copolymers showed a greater increase in E' after annealing. Fig. 15b shows a dramatic increase in E' around 500–700% for the HMW copolymer (1F) and 400–500% for the LMW copolymer (3D). In general, a larger increase in the E' storage modulus was observed for HMW polymers after annealing.

Fig. 16a and b compares the energy dampening behavior of the pure polymers that were quenched and annealed. For the pure homopolymers (Fig. 16a), it seems that annealing can increase the energy dampening of the LMW homopolymer and decrease the energy dampening of the HMW homopolymer. Fig. 16b shows the behavior of the copolymers under quenched and annealed conditions.

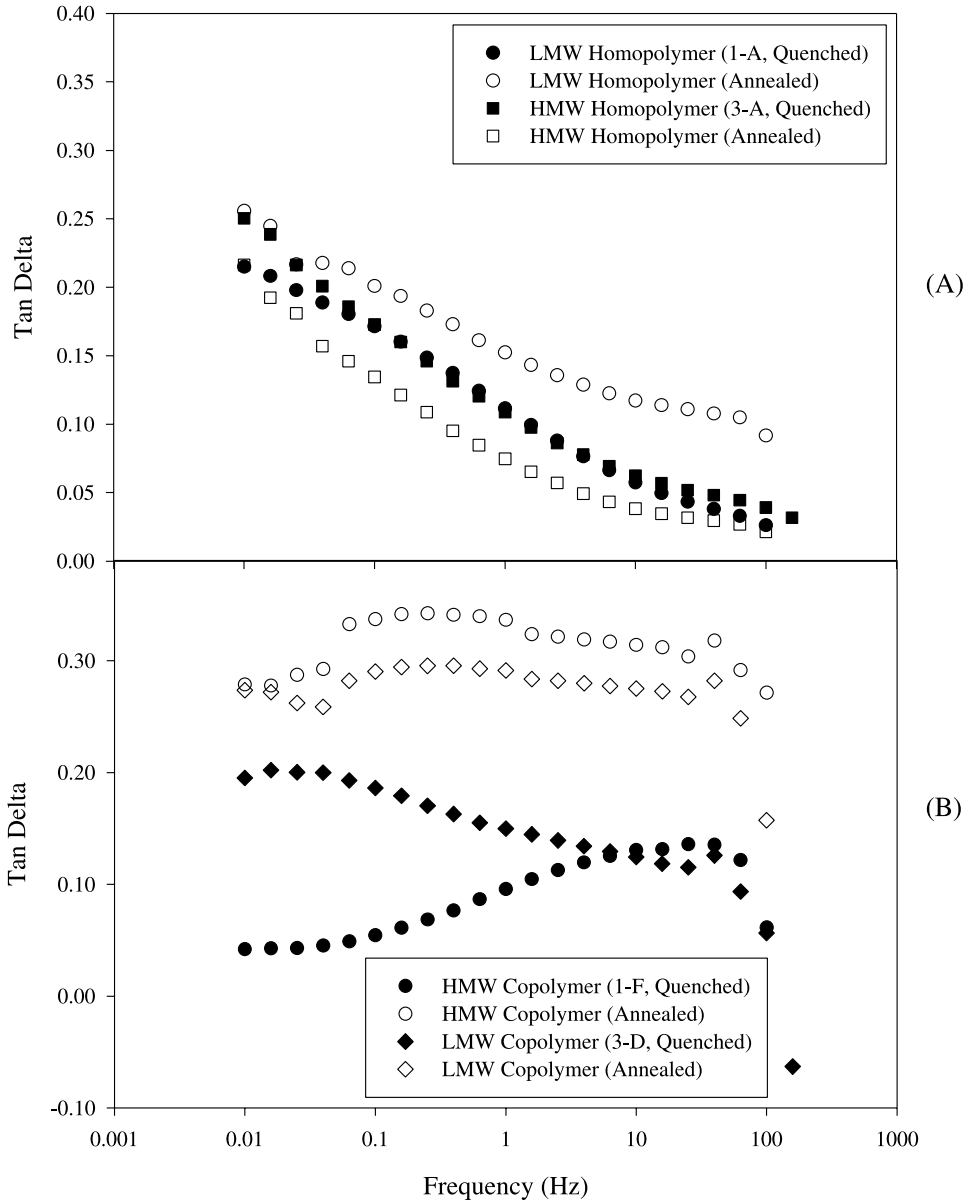

Fig. 16. Comparison of energy dampening between quenched and annealed polymers.

Overall, the energy dampening abilities of the copolymers increased greatly after annealing. Interestingly, the frequency dependence of the energy dampening behavior of the copolymers was also altered. For the HMW copolymer sample, it was observed earlier that the tan delta increased with increasing frequency. This behavior was believed to be the result of the low degree of crystallinity of the sample. However, after annealing, the tan delta of this HMW copolymer increases to a higher level and becomes frequency independent. This same independence was also observed for the annealed LMW copolymer. These observed changes after annealing demonstrate how the thermal history of a polymer can influence its frequency-dependent properties.

Fig. 17 shows the temperature dependence of the dynamic mechanical responses of the annealed HMW copolymer. As expected, the E' of the annealed HMW copolymer is greater than the quenched sample (above room temperature (Fig. 17a)). Examining the tan delta behavior (Fig. 17b), the quenched HMW copolymer exhibits a large β-transition but lacks an α-transition, possibly due to its low degree of crystallinity and small crystallite thickness. However, after annealing the HMW copolymer, an α-transition was observed. This provides some evidence that the alpha transition of the quenched copolymer was superimposed with the beta transition. During the annealing process, thicker crystal lamellae are formed which resulted in an increase in the

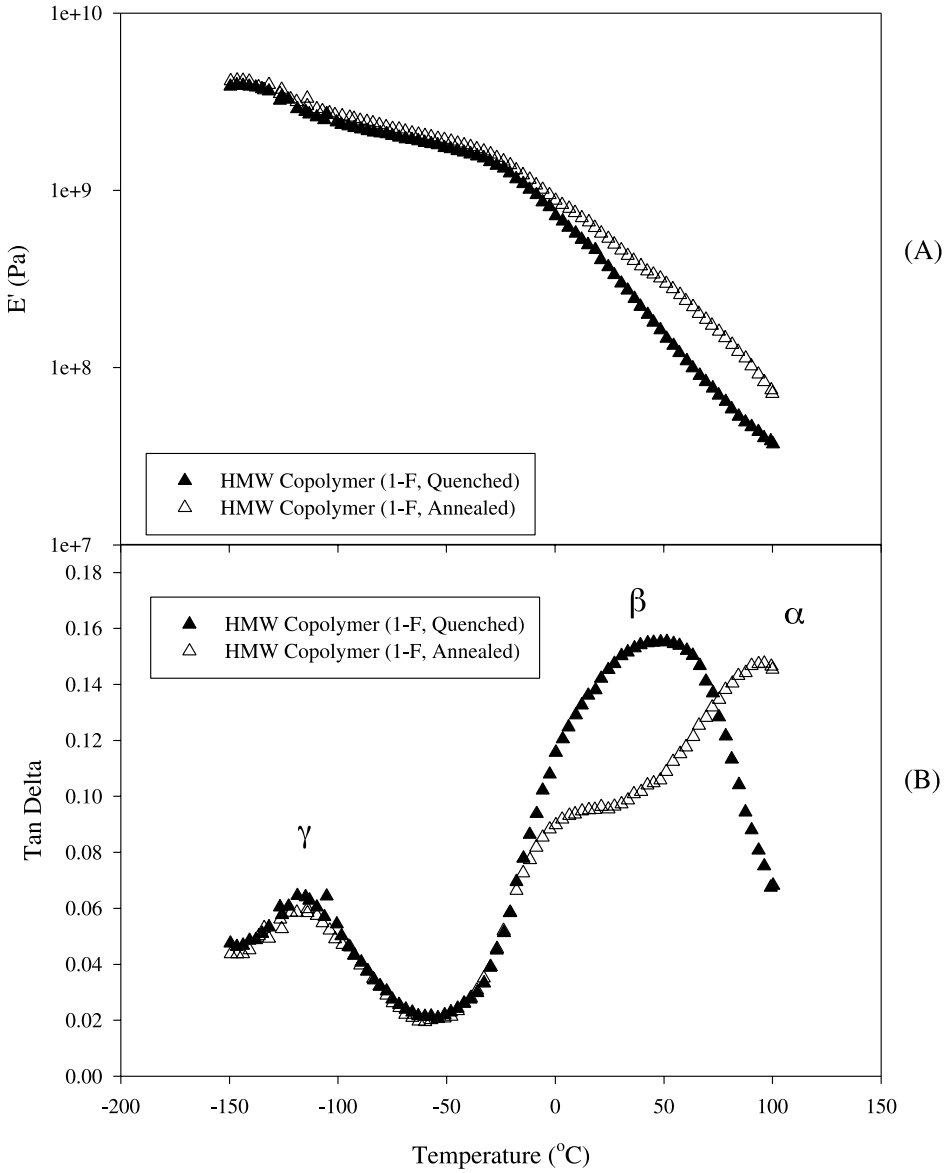

Fig. 17. Temperature dependence of dynamic response of a quenched and annealed copolymer.

alpha transition temperature. These observations are similar to Bensason et al. that reported that the α transition for LLDPE-like copolymers has a strong dependence on thermal history [8]. Faster cooling rates decrease the α transition temperature. The decrease in transition temperature was attributed to poorer crystal surface order, rather than to changes in lamellar thickness or the amount of crystallinity. Regardless, it has been demonstrated how the thermal treatment of a polymer changes the underlying crystal structure to directly influence the frequency dependence of its elastic and energy dampening properties.

Overall, it has been shown that the tensile and dynamic mechanical properties of poly(ethylene-*co*-1-octene) blends are highly influenced by the underlying microstructure, desired application (testing conditions) and thermal treatment (processing conditions).

4. Conclusions

Reactor blends of polyethylene and poly(ethylene-*co*-1-octene) with bimodal structural distributions were successfully produced via a two-step polymerization process. The microstructural characterization of these blends indicates that both the molecular weight and comonomer distributions are consistent with the method of polymerization. The physical properties of the blends containing LMW homopolymer/HMW copolymer and HMW homopolymer/LMW copolymer are consistent with the nature of their individual

components. For the tensile properties, the stiffness decreases with increasing fraction of the copolymer, regardless of the molecular weight of the homopolymer fraction. It was confirmed that the degree of crystallinity governs the stiffness of the polymer independently of MWD and SCBD details. However, the energy dampening properties of the polymers do benefit from the presence of the copolymer. Depending on the desired application, a balance of stiffness and toughness can be obtained by altering the composition of the blends. For some blends, the presence of HMW homopolymer can dominate the tensile properties showing little variation in the stiffness with the increased addition of copolymer.

It was also shown that the testing conditions and thermal treatment of a polymer greatly influence the resulting elastic and energy dampening properties. Depending on the desired application, annealing these polymers (especially very low density copolymers) can increase the stiffness of the polymers but also change the frequency response of the dynamic mechanical properties.

Overall, it has been demonstrated that reactor blends of LMW homopolymer/HMW copolymer and HMW homopolymer/LMW copolymer can exhibit a wide range of physical properties. Depending on the desired application, the tensile and dynamic mechanical properties of the blends can be tailored by controlling the fractions of individual components in the blend.

References

[1] Elvers B, Hawkins S, Schulz G. Ullman's encyclopedia of industrial chemistry, 5th ed. New York: VCH Publishers; 1992. p. 487–576.

[2] Foster GN, Wasserman SH. Metallocene and gas phase polymerization: molecular engineering pathway for advantaged polyethylene products, Metcon, Houston, TX; 1997.

[3] Hamielec AE, Soares JBP. Prog Polym Sci 1996;21:651–706.

[4] Avela A, Karling R, Takarhu J. Dcheme Monogr 1998;134:3–23.

[5] Martin JR, Johnson JF, Cooper AR. J Macromol Sci-Rev, Macromol Chem 1972;C8(1):57–199.

[6] Nunes RW, Martin JR, Johnson JF. Polym Engng Sci 1982;222: 205–28.

[7] Kale L, Plumley T, Patel R, Redwine O, Jain P. J Plast Film Sheet 1995;12:27–40.

[8] Bensason S, Minick J, Moet A, Chum S, Hiltner A, Baer E. J Polym Sci: Part B: Polym Phys 1996;34:1301–15.

[9] Utracki LA. Polymer alloys and blends, thermodynamics and rheology. New York: Hanser Publishers; 1990. p. 1–27.

[10] Berthold J, Bohm LL, Enderle HF, Gobel P, Luker H, Lecht R, Schulte U. Plast, Rubber Compos Process Appl 1996;25:368–72.

[11] Scheirs J, Bohm L, Boot J, Leevers PS. Trends Polym Sci 1996;4: 408–15.

[12] Bohm LL, Berthold J, Enderle HF, Fleissner M. Metalorganic catalysts for synthesis and polymerization: recent results by Ziegler–Natta and metallocene investigations. New York: Springer; 1999. p. 3–13.

[13] Chu KJ, Soares JBP, Penlidis A. J Polym Sci: Part A: Polym Chem 2000;38:462–8.

[14] Chu KJ, Li Pi Shan C, Soares JBP, Penlidis A. Macromol Chem Phys 1999;200:2372–6.

[15] Soares JBP, Monrabal B, Nieto J, Blanco J. Macromol Chem Phys 1998;199:1917–27.

[16] Xu X, Xu J, Feng K, Chen W. J Appl Polym Sci 2000;77:1709–15.

[17] Soares JBP, Kim JD. J Polym Sci: Part A: Polym Chem 2000;38: 1408–16.

[18] Blom R, Dahl IM. Macromol Chem Phys 1999;200:442–9.

[19] Cho K, Lee BH, Hwang KM, Lee H, Choe S. Polym Engng Sci 1998; 38(12):1969–75.

[20] Simanke AG, Galland GB, Neto RB, Quijada R, Mauler RS. J Appl Polym Sci 1999;74:1194–200.

[21] Grahm JT, Alamo RG, Mandelkern L. J Polym Sci: Part B: Polym Phys 1997;35:213–23.

[22] Brooks NWJ, Duckett RA, Ward IM. Polymer 1999;40:7367–72.

[23] Menard KP. Dynamic mechanical analysis—a practical introduction. New York: CRC Press; 1999. p. 151–62.

[24] Nitta KH, Tanaka A. Polymer 2000;42:1219–26.

[25] Simanke AG, Galland GB, Freitas L, da Jornada JAH, Quijada R, Mauler RS. Polymer 1999;40:5489–95.

[26] Kim YS, Chung CI, Lai SY, Hyun KS. J Appl Polym Sci 1996;59: 125–37.

[27] Sperling LH. Introduction to physical polymer science. Toronto: Wiley; 1990. p. 328.

[28] Mark JE, Eisenberg A, Graessley WW, Mandelkern L, Samulski ET, Koenig JL, Wignall GD. Physical properties of polymers, 2nd ed. Washington: ACS; 1993. Chapter 4.